ELSEVIER

PII: S0267-7261(97)00037-7

Soil Dynamics and Earthquake Engineering **17** (1998) 269–277

Printed in Great Britain
0267-7261/98/$19.00+0.00

Two dimensional transient fundamental solution due to suddenly applied load in a half-space

F. Guan[a], I. D. Moore[a] & C. C. Spyrakos[b,*]

[a]*Department of Civil Engineering, University of Western Ontario, London, Ontario N6A 5B9, Canada*
[b]*Department of Civil Engineering, National Technical University of Athens, Zografos 15700, Greece*

(Received 1 July 1996; accepted 4 August 1997)

A transient Green function due to suddenly applied line loads in an isotropic and homogeneous half-space is reported in this paper. The derivation of the half-space Green function in the Laplace and the Fourier transform spaces is first reviewed. Following an explicit inversion of the Fourier transform, the inverse Laplace transform is implemented along the contour integral on the p-complex plane in an integral form. The half-space Green function consists of full-space Green functions and a singularity-free complementary term. It can be easily incorporated into current transient boundary elements using the transient full-space Green function. Combined with finite elements, the half-space Green function can be used in a hybrid procedure to solve transient half-space problems without discretization of the free surface. Numerical results are presented to illustrate transient wave propagation in a half-space. © 1998 Published by Elsevier Science Ltd. All rights reserved

1 INTRODUCTION

In recent years, the boundary element method (BEM) has received increasing attention in solving dynamic problems involving unbounded media (e.g. Refs [1–3]). The fundamental solution since all these formulations were Green functions for a full-space medium. In order to solve half-space problems, a part of the free surface has to be discretized in the vicinity of the region of interest to satisfy the traction-free conditions. Availability of half-space fundamental solutions eliminates the use of traction-free surface and greatly simplifies the solution procedure. Many researchers have therefore attempted to derive fundamental solutions for the half-space problem. Lamb[4] and de Hoop[5] obtained solutions for surface line loading. Apsel[6] and Kausel[7] respectively developed Green's functions for a layered half-space in the frequency domain. The surface response due to the impulsive line load within a half-space is presented by Payton[8] using de Hoop's technique. A transient solution to the impulsive point load has been given by Johnson[9]. Kobayashi and Nishimura[10] discussed the derivation of a half-space fundamental solution based on the full-space one. A two-dimensional frequency domain solution for a half-space has been developed by Kobayashi[11]. Banerjee and Mamoon[12] derived the half-space solution for the periodic point force using a technique developed by Mindlin[13] who solved the corresponding 3-D static problem. Guan and Novak[14,15] developed transient Green functions due to surface loads over rectangular and strip regions respectively.

The direct time domain BEM has become an attractive alternative to the frequency domain BEM for solving non-linear problems. This paper describes the derivation of a transient fundamental solution due to line loads suddenly applied *within* the half-space. Utilising the solution in the frequency and wave-number domains given by Kobayashi[11], the time domain solution is obtained after first inverting the Laplace transform in an integral form following the procedure of Eason[16]. The inversion of the Fourier transform is then carried out explicitly with respect to the wave-number ξ. Other applications of this technique can be found in studies of Guan and Novak[14,15], who obtained three-dimensional solutions for surface loading. Numerical results are presented to illustrate wave propagations in the half-space.

*Corresponding author. Address: National Technical University of Athens, Civil Engineering Department, Zografos 15700, Greece.

2 FORMULATION OF THE PROBLEM

Consider an elastic, homogeneous half-space described by the shear modulus μ, mass density ρ and Poisson's ratio ν, shown in Fig. 1. The longitudinal, transverse and Rayleigh wave velocities are denoted by α, β and C_R. Based on Stokes' solution (see e.g. Ref.[17]), the Green function for an infinite medium subjected to suddenly applied line loads can be expressed in the Laplace transform domain as

$$\Gamma^*_{jk} = \frac{1}{2\pi\mu p}\left(\frac{\beta^2}{p^2}\frac{\partial^2}{\partial^2 x_j x_k}\left(K_0\left(\frac{p}{\alpha r}\right) - K_0\left(\frac{p}{\beta r}\right)\right) + \delta_{jk}K_0\left(\frac{p}{\beta r}\right)\right) \tag{1}$$

where $x_1 = x$, $x_2 = z$, as in the coordinate system, Fig. 1. The superscript $*$ denotes the Laplace transform with respect to time, K_0 the modified Bessel function, p the Laplacian parameter and

$$r = \sqrt{x^2 + (z-\zeta)^2} \tag{2}$$

The loads are applied at the point with coordinates $(0,\zeta)$ as shown in Fig. 2.

Based on the following expression for the modified Bessel function K_0 [18]

$$K_0(k(x^2+y^2)^{1/2}) = \int_0^\infty \exp(-y(k^2+\xi^2)^{1/2})\frac{\cos x\xi}{(k^2+\xi^2)^{1/2}}\mathrm{d}\xi \tag{3}$$

$$\mathrm{Re}(y) > 0,\ \mathrm{Re}(k) > 0$$

we have

$$\int_0^\infty K_0(k(x^2+y^2)^{1/2})\mathrm{e}^{\mathrm{i}\xi x}\,\mathrm{d}\xi = \frac{\pi\exp(-y(k^2+\xi^2)^{1/2})}{(k^2+\xi^2)^{1/2}} \tag{4}$$

Utilising eqns (1) and (4), the displacement expressions in the Fourier transform domain with respect to the coordinate x can be obtained

$$\bar{\Gamma}^*_{xx}(\xi,z,p;\zeta) = \int_{-\infty}^{+\infty}\Gamma^*_{xx}(x,z,p;\zeta)\mathrm{e}^{\mathrm{i}\xi x}\,\mathrm{d}x = \frac{1}{2\rho p^3 k_\alpha}(\xi^2\mathrm{e}^{(z-\zeta)k_\alpha} - k_\alpha k_\beta \mathrm{e}^{(z-\zeta)k_\beta}) \tag{5a}$$

$$\bar{\Gamma}^*_{zz}(\xi,z,p;\zeta) = \int_{-\infty}^{+\infty}\Gamma^*_{zz}(x,z,p;\zeta)\mathrm{e}^{\mathrm{i}\xi x}\,\mathrm{d}x = \frac{1}{2\rho p^3 k_\beta}(\xi^2\mathrm{e}^{(z-\zeta)k_\beta} - k_\alpha k_\beta \mathrm{e}^{(z-\zeta)k_\alpha}) \tag{5b}$$

$$\bar{\Gamma}^*_{xz}(\xi,z,p;\zeta) = \int_{-\infty}^{+\infty}\Gamma^*_{xz}(x,z,p;\zeta)\mathrm{e}^{\mathrm{i}\xi x}\,\mathrm{d}x = \frac{-\mathrm{i}\xi}{2\rho p^3}(\mathrm{e}^{(z-\zeta)k_\beta} - \mathrm{e}^{(z-\zeta)k_\alpha}) \tag{5c}$$

$$\bar{\Gamma}^*_{zx}(\xi,z,p;\zeta) = \bar{\Gamma}^*_{xz}(\xi,z,p;\zeta) \tag{5d}$$

where the bar denotes the Fourier transform with respect to the horizontal coordinate, and the variables k_α and k_β are given by

$$k_\beta = \sqrt{\xi^2 + p^2/\beta^2} \tag{6a}$$

$$k_\alpha = \sqrt{\xi^2 + p^2/\alpha^2} \tag{6b}$$

The stress components can be obtained from the stress–displacement relationship

$$\tau^n_{jk} = \lambda\Gamma_{mn,m}\delta_{jk} + \mu(\Gamma_{jn,k} + \Gamma_{kn,j}) \tag{7}$$

where the index n denotes the stress induced by the force in the nth direction, and λ and μ are Lame's constants.

The displacement fundamental solution for the half-space can be determined using fictitious forces shown in Fig. 2 based on the solution for the full-space. The solution has been described in detail by Kobayashi[11] and only the salient steps are presented in the following.

For the loads applied shown in Fig. 2(a), only the traction component t_{zz} is induced at the plane $z = 0$; while for the loads in Fig. 2(b), only the traction component t_{zx} is induced at the plane $z = 0$. In order to satisfy the traction-free conditions

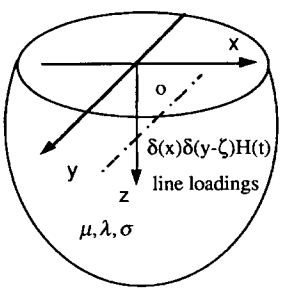

Fig. 1. Geometry of the problem.

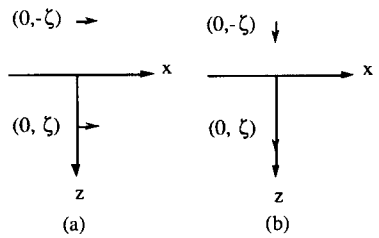

Fig. 2. Illustration of the method involving fictitious forces.

at $z=0$, tractions opposite in direction but equal in magnitude must be applied at $z=0$. Therefore, the Green function for a half-space consists of the displacements induced by the two line loads and the tractions applied at the surface, viz.

$$\bar{G}^*_{jk}(\xi,z,p;\zeta)=\bar{\Gamma}^*_{jk}(\xi,z,p;\zeta)+\bar{\Gamma}^*_{jk}(\xi,z,p;-\zeta)+\bar{u}^*_{jk}(\xi,z,p\,\zeta) \tag{8}$$

and where

$$\bar{u}^*_{xx}=\frac{\xi^2}{\rho\Delta_R k_\alpha p^3}\left(2k_\alpha k_\beta e^{-k_\beta z}-\left(2\xi^2+\frac{p^2}{\beta^2}\right)e^{-k_\alpha z}\right)\times\left(2k_\alpha k_\beta e^{-k_\beta \zeta}-\left(2\xi^2+\frac{p^2}{\beta^2}\right)e^{-k_\alpha \zeta}\right) \tag{9a}$$

$$\bar{u}^*_{zx}=\frac{-i\xi}{\rho\Delta_R p^3}\left(2\xi^2 e^{-k_\beta z}-\left(2\xi^2+\frac{p^2}{\beta^2}\right)e^{-k_\alpha z}\right)\times\left(2k_\alpha k_\beta e^{-k_\beta \zeta}-\left(2\xi^2+\frac{p^2}{\beta^2}\right)e^{-k_\alpha \zeta}\right) \tag{9b}$$

$$\bar{u}^*_{xz}=\frac{i\xi}{\rho\Delta_R p^3}\left(2\xi^2 e^{-k_\alpha z}-\left(2\xi^2+\frac{p^2}{\beta^2}\right)e^{-k_\beta z}\right)\times\left(2k_\alpha k_\beta e^{-k_\alpha \zeta}-\left(2\xi^2+\frac{p^2}{\beta^2}\right)e^{-k_\beta \zeta}\right) \tag{9c}$$

$$\bar{u}^*_{zz}=\frac{\xi^2}{\rho\Delta_R k_\beta p^3}\left(2k_\alpha k_\beta e^{-k_\alpha z}-\left(2\xi^2+\frac{p^2}{\beta^2}\right)e^{-k_\beta z}\right)\times\left(2k_\alpha k_\beta e^{-k_\alpha \zeta}-\left(2\xi^2+\frac{p^2}{\beta^2}\right)e^{-k_\beta \zeta}\right) \tag{9d}$$

where

$$\Delta_R=\left(\frac{p^2}{\beta^2}+2\xi^2\right)-4\xi^2 k_\alpha k_\beta \tag{10}$$

is the Rayleigh function.

Applying the inverse Laplace and Fourier transforms to eqns (8)–(9), we obtain

$$G_{jk}(x,z,t;\zeta)=\Gamma_{jk}(x,z,t;\zeta)+\Gamma_{jk}(x,z,t;-\zeta)+u_{jk}(x,z,t;\zeta) \tag{11}$$

where the first two terms are Stokes' solutions. Stoke's solution for the line load with a Heaviside time step function is given by (see Ref.[17])

$$\Gamma_{jk}=\frac{1}{2\pi\rho}\frac{\partial^2}{\partial x_j x_k}\left(\int_r^\infty\frac{d\eta}{(\eta^2-r^2)^{1/2}}\int_0^\infty \nu\left(H\left(t\frac{\eta}{\alpha}-\nu\right)-H\left(t\frac{\eta}{\beta}-\nu\right)\right)d\nu+\frac{\delta_{jk}}{\beta^2}\int_r^\infty H\left(t-\frac{\eta}{\beta}\right)\frac{d\eta}{(\eta^2-r^2)^{1/2}}\right) \tag{12}$$

The third term on the right hand side of eqn (11) is expressed as

$$u_{jk}(x,z,t;\zeta)=\frac{1}{2\pi}\int_{-\infty}^{+\infty}\bar{u}_{jk}(\xi,z,t;\zeta)e^{-i\xi x}\,d\xi \tag{13}$$

where $\bar{u}_{jk}(\xi,z,t;\zeta)$ is obtained by the contour integration on the p-complex plane from the expressions in eqn (9). As demonstrated in Appendix A, the wave-number ξ in $\bar{u}_{jk}(\xi,z,t;\zeta)$ is separated from other variables and the inverse Fourier transform can be implemented explicitly. The expressions used in the evaluation of the integration in eqn (13) are defined as (see Ref.[18])

$$\chi_1(\gamma,y)=\int_0^\infty\frac{e^{-\xi\gamma}\sin(\xi y)\sin^2(\xi\eta t/2)}{\xi}d\xi=\frac{1}{2}\arctan\frac{y}{\gamma}-\frac{1}{4}\arctan\frac{2\gamma y}{\gamma^2+\eta^2t^2-y^2} \tag{14a}$$

$$\chi_2(\gamma,y)=\int_0^\infty\frac{e^{-\xi\gamma}\cos(\xi y)\sin^2(\xi\eta t/2)}{\xi}d\xi=\frac{1}{8}\ln\frac{(\gamma^2+(\eta t+y)^2)(\gamma^2+(\eta t-y)^2)}{(\gamma^2+y^2)^2} \tag{14b}$$

$$\chi_3(y)=\int_0^\infty\frac{\sin(\xi y)\sin^2(\xi\eta t/2)}{\xi}d\xi=\begin{cases}\frac{\pi}{4} & 0<y<\eta t\\ 0 & y>\eta t\end{cases} \tag{14c}$$

$$\chi_4(y)=\int_0^\infty\frac{\cos(\xi y)\sin^2(\xi\eta t/2)}{\xi}d\xi=\frac{1}{4}\ln\left|\frac{y^2-\eta^2t^2}{y^2}\right| \tag{14d}$$

Substituting eqn (14) into eqn (13) results in eqns (15). The various parameters in eqn (15) are given in Appendix A. An adaptive integration scheme has been used to evaluate the integrals in eqn (15)[19]. It is straightforward to integrate the Green function and implement it in existing BEM codes (Richter and Schmid[20] describe procedures for treating special cases associated with surface elements).

3 NUMERICAL ILLUSTRATIONS

In this section, the wave propagation characteristics in the half-space are investigated using the Green function developed in this work. The Poisson's ratio for the half-space is $\nu = 0{\cdot}25$.

Lamb[4] studied the surface response due to a vertical impulsive load. A complete solution has been presented by de Hoop[5] using a transform technique, including the response to an impulsive load applied in the horizontal direction. The time dependence of their solutions is the Dirac delta function. The response at the observation point $(r,0)$ due to the load applied on the surface at position (0,0)

$$u_{xx}\frac{-(4c_\alpha^2c_\beta^2\chi_2(c_\beta(z+\zeta),x)-2c_\alpha c_\beta c_R(\chi_2(c_\alpha z+c_\beta\zeta),x)+\chi_2(c_\beta z+c_\alpha\zeta),x))+c_R^2\chi_2(c_\alpha(z+\zeta),x)}{\pi\rho K(C_R)c_\alpha}$$

$$+\int_\beta^\alpha\sum_{j=0}^{1}\frac{2c^2(4a^2b^2\chi_3(b(z+\zeta)+x_j)-2abc(\chi_2(az,b\zeta+x_j)+\chi_2(a\zeta,bz+x_j))}{\pi^2\rho a((2-\eta^2/\beta^2)^4+16(\eta^2/\beta^2-1)(1-\eta^2/\alpha^2))\eta^3}\mathrm{d}\eta$$

$$-8\int_\beta^\alpha\sum_{j=0}^{1}\frac{b(4a^2b^2\chi_4(b(z+\zeta)+x_j)+2abc(\chi_1(az,x_j+b\zeta)+\chi_1(a\zeta,x_j+bz)-c^2\chi_2(a(z+\zeta),x))}{\pi^2\rho((2-\eta^2/\beta^2)^4+16(\eta^2/\beta^2-1)(1-\eta^2/\alpha^2))\eta^3}\mathrm{d}\eta$$

$$-2\int_\beta^\infty\sum_{j=0}^{1}\frac{4a^2b^2\chi_4(x_j+b(z+\zeta))-2abc(\chi_4(x_j+bz+a\zeta)+\chi_4(x_j+az+b\zeta))+c^2\chi_4(x_j+a(z+\zeta))}{\pi^2\rho a((2-\eta^2/\beta^2)^2+4\sqrt{(\eta^2/\beta^2-1)(\eta^2/\alpha^2-1)})\eta^3}\mathrm{d}\eta \tag{15a}$$

$$u_{zx}\frac{-(4c_\alpha c_\beta\chi_1(c_\beta(z+\zeta),x)-2c_R(\chi_1(c_\beta z+c_\alpha\zeta),x)+c_\alpha c_\beta\chi_1(c_\alpha z+c_\beta\zeta),x))+c_R^2\chi_1(c_\alpha(z+\zeta),x)}{\pi\rho K(C_R)}$$

$$-\int_\beta^\alpha\sum_{j=0}^{1}(-1)^j\frac{2c^2(4ab\chi_3(b(z+\zeta)+x_j)-2c(\chi_2(a\zeta,bz+x_j)+ab\chi_1(az,b\zeta+x_j))}{\pi^2\rho a((2-\eta^2/\beta^2)^4+16(\eta^2/\beta^2-1)(1-\eta^2/\alpha^2))\eta^3}\mathrm{d}\eta$$

$$+8\int_\beta^\alpha\sum_{j=0}^{1}(-1)^j\frac{ab(4ab\chi_4(b(z+\zeta)+x_j)+2c(\chi_1(a\zeta,x_j+bz)-ab\chi_2(az,x_j+b\zeta)-c^2\chi_1(a(z+\zeta),x_j))}{\pi^2\rho((2-\eta^2/\beta^2)^4+16(\eta^2/\beta^2-1)(1-\eta^2/\alpha^2))\eta^3}\mathrm{d}\eta$$

$$+2\int_\beta^\infty\sum_{j=0}^{1}(-1)^j\frac{4ab\chi_4(x_j+b(z+\zeta))+2c(\chi_4(x_j+(bz+a\zeta))-ab\chi_4(x_j+(az+b\zeta)))-c^2\chi_4(x_j+a(z+\zeta))}{\pi^2\rho((2-\eta^2/\beta^2)^2+4\sqrt{(\eta^2/\beta^2-1)(\eta^2/\alpha^2-1)})\eta^3}\mathrm{d}\eta \tag{15b}$$

$$u_{zz}\frac{-(4c_\alpha^2c_\beta^2\chi_2(c_\alpha(z+\zeta),x)-2c_\alpha c_\beta c_R(\chi_2(c_\alpha z+c_\beta\zeta),x)+\chi_2(c_\beta z+c_\alpha\zeta),x))+c_R^2\chi_2(c_\beta(z+\zeta),x)}{\pi\rho K(C_R)c_\alpha}$$

$$+\int_\beta^\alpha\sum_{j=0}^{1}\frac{2c^2(4a^2b^2\chi_2(a(z+\zeta),x)+2abc(\chi_1(az,b\zeta+x_j)+\chi_1(a\zeta,bz+x_j)-c^2\chi_4(b(z+\zeta)+x_j))}{\pi^2\rho b((2-\eta^2/\beta^2)^4+16(\eta^2/\beta^2-1)(1-\eta^2/\alpha^2))\eta^3}\mathrm{d}\eta$$

$$-8\int_\beta^\alpha\sum_{j=0}^{1}\frac{a(c^2\chi_3(b(z+\zeta)+x_j)+2abc(\chi_1(az,x_j+b\zeta)+\chi_1(a\zeta,x_j+bz))}{\pi^2\rho((2-\eta^2/\beta^2)^4+16(\eta^2/\beta^2-1)(1-\eta^2/\alpha^2))\eta^3}\mathrm{d}\eta$$

$$-2\int_\beta^\infty\sum_{j=0}^{1}\frac{4a^2b^2\chi_4(x_j+a(z+\zeta))+2abc(\chi_4(x_j+(bz+a\zeta))+\chi_4(x_j+(az+b\zeta)))+c^2\chi_4(x_j+b(z+\zeta))}{\pi^2\rho b((2-\eta^2/\beta^2)^2+4\sqrt{(\eta^2/\beta^2-1)(\eta^2/\alpha^2-1)})\eta^3}\mathrm{d}\eta \tag{15c}$$

$$u_{xz}\frac{-(4c_\alpha c_\beta\chi_1(c_\alpha(z+\zeta),x)-2c_R(\chi_1(c_\alpha z+c_\beta\zeta),x)+c_\alpha c_\beta\chi_1(c_\beta z+c_\alpha\zeta),x))+c_R^2\chi_1(c_\beta(z+\zeta),x)}{\pi\rho K(C_R)c_\alpha}$$

$$+\int_\beta^\alpha\sum_{j=0}^{1}(-1)^j\frac{2c^2(4ab\chi_1(a(z+\zeta),x_j)-2c(\chi_2(az,b\zeta+x_j)+ab\chi_1(a\zeta,bz+x_j)+c^2\chi_4(b(z+\zeta)+x_j))}{\pi^2\rho((2-\eta^2/\beta^2)^4+16(\eta^2/\beta^2-1)(1-\eta^2/\alpha^2))\eta^3}\mathrm{d}\eta$$

$$+8\int_\beta^\alpha\sum_{j=0}^{1}(-1)^j\frac{b(c^2\chi_3(b(z+\zeta)+x_j)-2c(\chi_1(az,x_j+b\zeta)-ab\chi_2(a\zeta,x+b_jz))}{\pi^2\rho((2-\eta^2/\beta^2)^4+16(\eta^2/\beta^2-1)(1-\eta^2/\alpha^2))\eta^3}\mathrm{d}\eta$$

$$-2\int_\beta^\infty\sum_{j=0}^{1}(-1)^j\frac{4ab\chi_4(x_j+a(z+\zeta))+2c(\chi_4(x_j+(az+b\zeta))-ab\chi_4(x_j+(bz+a\zeta)))-c^2\chi_4(x_j+b(z+\zeta))}{\pi^2\rho((2-\eta^2/\beta^2)^2+4\sqrt{(\eta^2/\beta^2-1)(\eta^2/\alpha^2-1)})\eta^3}\mathrm{d}\eta \tag{15d}$$

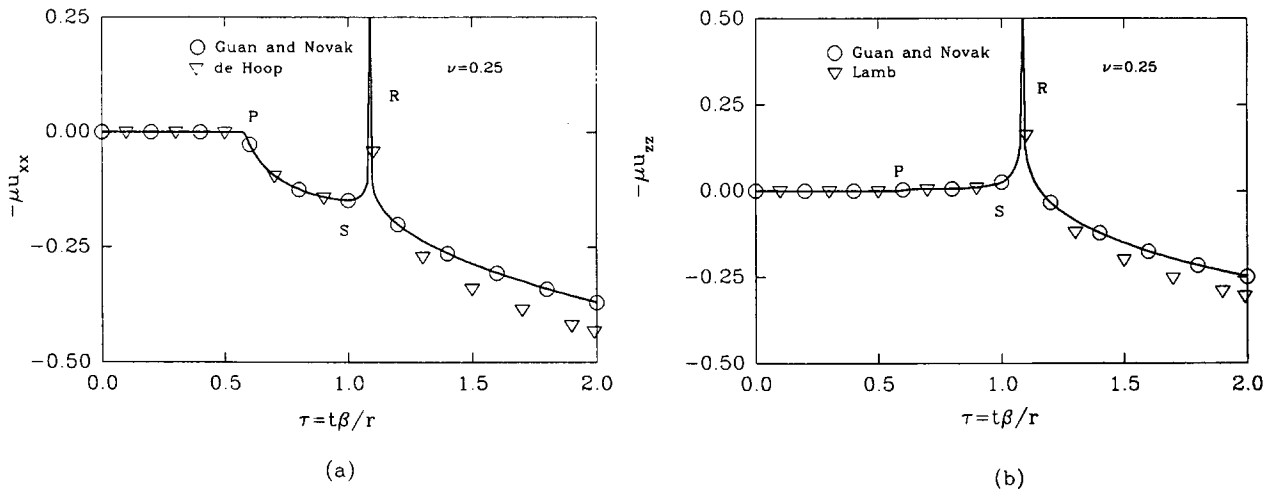

Fig. 3. Comparisons between the Green function and results from the literature.

is depicted in Fig. 3 versus the normalized time τ defined as $\tau = t\beta/r$, where r is the distance between the observation point and the source. Also, the solutions of Guan and Novak[15], Lamb[4] and de Hoop[5] are presented in Fig. 3 for the purpose of comparison. The results from de Hoop (Fig. 3(a)) and Lamb (Fig. 3(b)) were obtained with numerical time convolution using their original solutions. The arrival times of the longitudinal, transverse and Rayleigh waves are denoted by P, S and R. Excellent agreement among the results is observed before the Rayleigh wave arrives at the observation point. The results from Lamb and de Hoop start diverging from the other solutions after the Rayleigh wave arrives. The differences are induced by strong singularities in their original solutions used as integral kernels in the numerical time convolution.

As indicated in Fig. 3(a), the arrival of the P wave is evident in the response of u_{xx}. After the arrival of the S wave, the trend of the response changes. The singularity occurs as the Rayleigh wave arrives. The P wave arrival is not obvious in the displacement u_{zz} shown in Fig. 3(b). However, the arrival of the S wave can be clearly distinguished. The contribution from the Rayleigh wave is pronounced in the response around the time it arrives. After the Rayleigh wave leaves, both displacements u_{xx} and u_{zz} increase monotonically with the increasing time.

The effect of the wave reflection at the surface is plotted in Fig. 4 for various source burial depths, where ∞ represents the solution in the full-space. In this study, the distance between the source and the observation points is constant despite the changes in the burial depth of the source below the free surface. Fig. 4 shows the displacements in the directions of the applied loads. Before the reflected wave at the free surface arrives at the observation point, the responses are exactly the same. The solutions for the half-space subsequently deviate from the full-space solution. As the burial depth of the load increases, the difference between the half-space and full-space solutions narrows. It is observed that the wave reflection more significantly affects

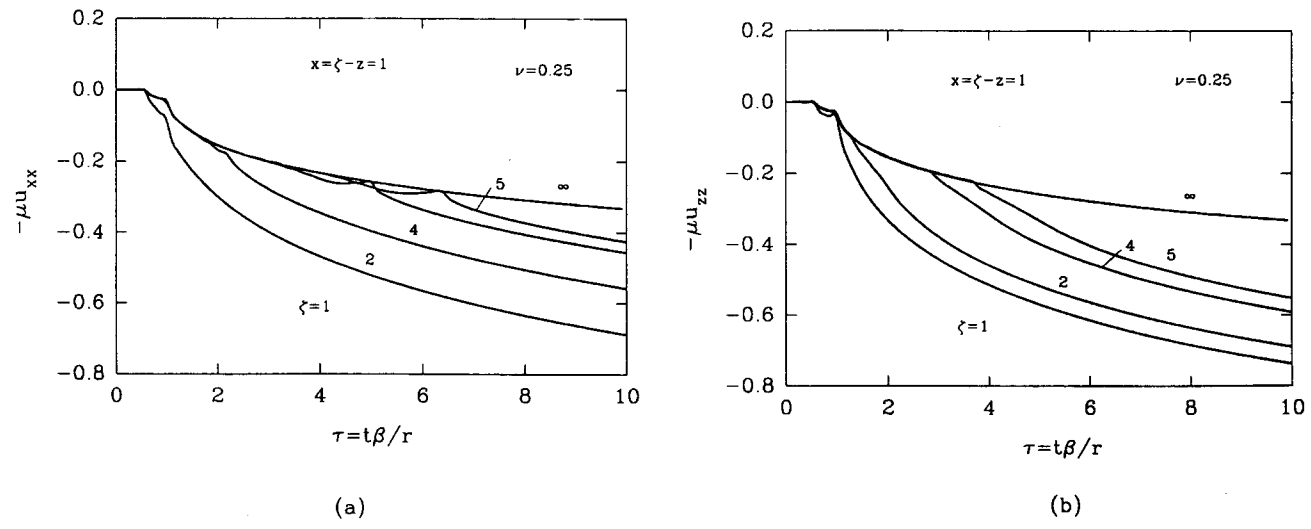

Fig. 4. Green function solution for displacement u_{ii} to loads at various depths below the free surface.

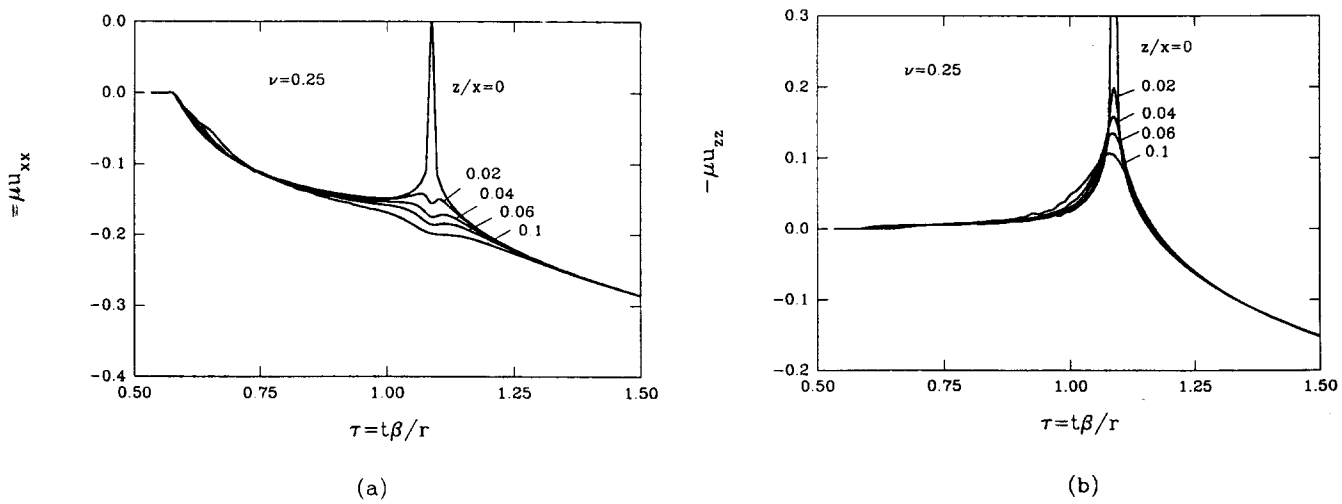

Fig. 5. Effect of the Rayleigh wave on the Green function for displacement u_{ii} at various observation points due to loads applied at the surface.

the displacement in the direction normal to the boundary of the half-space, i.e. in the z direction. The half-space solution yields greater displacement predictions that does the full-space solution, because of overlapping of the reflected waves. However, solutions not presented here reveal that the displacements u_{ij} $(i \neq j)$ in the half-space converge rapidly to those in the full-space as the depth of the observation point z increases.

The influence of the Rayleigh wave on the response induced by the surface load is depicted in Figs 5 and 6. Unlike the surface response, response u_{ii} $(i = x, z)$ within the half-space remains definite when the Rayleigh wave front arrive, Fig. 5. The contribution from the Rayleigh wave decreases significantly as the depth of the observation point z increases. The response u_{xx} within the half-space for $z/x = 0{\cdot}1$ drops slightly as the Rayleigh wave arrives. It appears that the u_{zz} response is more significantly affected by the Rayleigh wave.

Fig. 6 shows the response u_{ij} $(i \neq j)$ for different observation points in the half-space. Each of the surface responses feature finite jumps after the Rayleigh wave arrives. However, for the observation points below the surface, the influence of the Rayleigh wave is not evident. The arrival of the S wave is marked, particularly for the observation points deeper below the free surface.

4 CONCLUDING REMARKS

A transient Green function has been developed for half-space response to suddenly applied line loads. It can be readily implemented in hybrid finite element–boundary element formulations to solve transient elastodynamic problems without modeling of the free surface. The Green function can be used to construct transient boundary elements for problems in elastodynamics involving a half-space. The

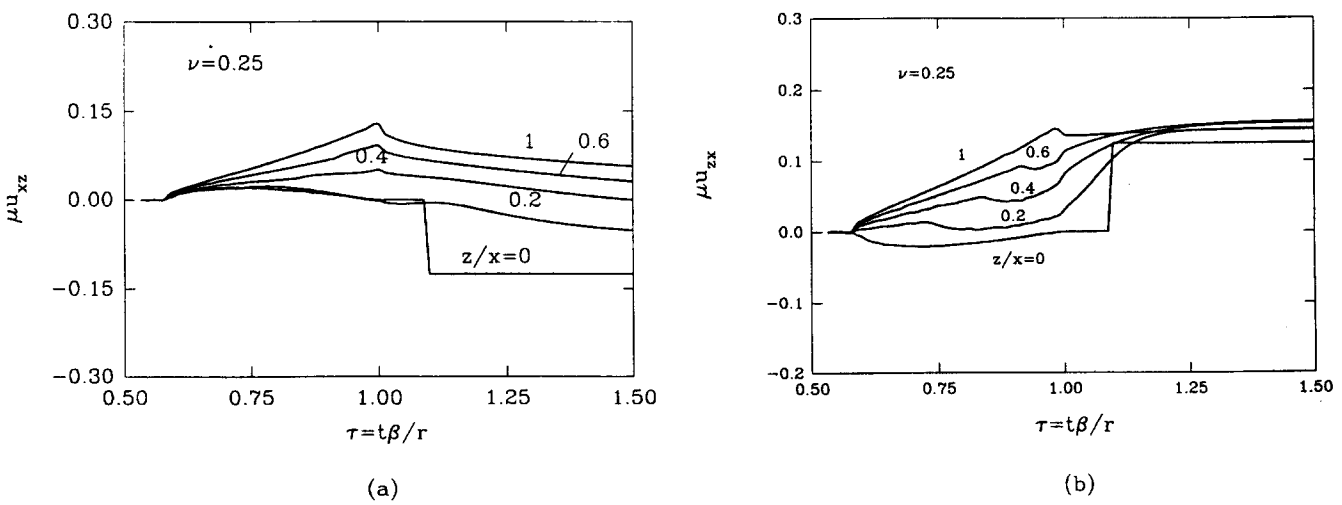

Fig. 6. Effect of the Rayleigh wave on the Green function for displacement u_{ij} $(i \neq j)$ at various observation points due to loads applied at the surface.

procedure used to derive the fundamental solution can be extended to three dimensions. Comparisons with other solutions confirmed the accuracy of the transient Green function. Illustrative numerical results from transient wave propagation in a half-space have been presented.

ACKNOWLEDGEMENTS

Support for this work has been provided through research and equipment grants to the first author from the Natural Sciences and Engineering Research Council of Canada.

REFERENCES

1. Spyrakos, C. C. and Beskos, D. E. Dynamic response of flexible strip-foundations by boundary and finite elements. *Soil Dyn. Earthq. Engng.*, 1986, **5**, 84–96.
2. Spyrakos, C. C. and Beskos, D. E. Dynamic response of rigid strip-foundations by time domain boundary element method. *Int. J. Numerical Methods Engng.*, 1986, **23**, 1547–1565.
3. Spyrakos, C. C., Strip-foundations. In *Boundary Element Techniques in Geomechanics*, Chapter 5. Elsevier, New York, 1993, 147–177.
4. Lamb, H. On the propagation of tremors on the surface of an elastic solid. *Philos. Trans. R. Soc., London, Ser. A*, 1904, **203**, 1–42.
5. de Hoop, A. T. The surface line source problem. *Appl. Sci. Res.*, 1960, **B8**, 349–356.
6. Apsel, R. J., Dynamic Green's functions for layered medium and applications to boundary value problems. Ph.D. Dissertation, University of California, San Diego, 1979.
7. Kausel, E., An explicit solution for the Green functions for dynamic loads in layered media. MIT Research Rep. R81-13, Cambridge, MA, 1981.
8. Payton, R. G. Transient motion of an elastic half-space due to moving surface line load. *Int. J. Engng. Sci.*, 1967, **5**, 49–79.
9. Johnson, L. R. Green's function for Lamb's Problem. *Geophys. J. R. Astron. Soc.*, 1974, **37**, 99–131.
10. Kobayashi, S. and Nishimura, N. Green's tensors for elastic half-space, an application to the boundary integral equation method. *Mem. Fac. Eng. Kyoto Univ.*, 1980, **XLII**, 228–241.
11. Kobayashi, S., Some problems of the boundary integral equation method in elastodynamics. In *Boundary Elements V*, ed. C. A. Brebbia *et al.* Springer, Berlin, 1983, pp. 775–784.
12. Banerjee, P. K. and Mamoon, S. M. A fundamental solution due to a periodic point force in the interior of an elastic half-space. *Earthq. Engng. Struct. Dyn.*, 1990, **19**, 91–105.
13. Mindlin, R. D. Force at a point in the interior of a semi-infinite solid. *J. Appl. Phys.*, 1936, **7**, 195–202.
14. Guan, F. and Novak, M. Transient response of a half-space due to rectangular impulsive loading. *J. Appl. Mech. ASME*, 1994, **61**, 256–263.
15. Guan, F. and Novak, M. Transient response of group rigid strip foundations due to impulsive loading. *Earthq. Engng. Struct. Dyn.*, 1994, **23**, 671–685.
16. Eason, G. On the torsional impulsive loading of an elastic half-space. *Q. J. Mech. Appl. Math.*, 1964, **17**, 279–292.
17. Eringen, A. C. & Suhibu, E. S., *Elastodynamics. Vol. II, Linear Theory*. Academic Press, New York, 1975.
18. Gradshtein, I. S. & Ryzhik, I. M., *Table of Integrals, Series and Products*. Academic Press, New York, 1980.
19. Clenshaw, C. W. and Curtis, A. R. A method for numerical integration on an automatic computer. *Numerical Math.*, 1960, **2**, 197–205.
20. Richter, C. & Schmid, G., A Green = 92s function of the elastodynamic half-plane and its application to the time domain BEM of elastodynamics. *Proc. BEM, 17*, Madison, WI, 1995.
21. Morse, P. M. & Feshbach, H., *Methods of Theoretical Physics*. McGraw-Hill, New York, 1953.

APPENDIX A

The $\bar{u}_{jk}$ can be obtained by contour integration on the p-complex plane using expressions such as

$$\bar{u}_{xx} = \frac{1}{2\pi i}\int_{\gamma-j\infty}^{\gamma+j\infty} \bar{u}^*_{xx} e^{pt}\, dp \tag{A1}$$

where

$$\bar{u}^*_{xx} = \frac{\xi^2}{\rho\Delta_R k_\alpha p^2}\left(2k_\alpha k_\beta e^{-k_\beta z} - \left(2\xi^2 + \frac{p^2}{\beta^2}\right)e^{-k_\alpha z}\right) \times \left(2k_\alpha k_\beta e^{-k_\beta \zeta}\left(2\xi^2 + \frac{p^2}{\beta^2}\right)e^{-k_\alpha \zeta}\right)$$

is an analytic complex function except at poles and branch points. The poles of the integrand in eqn (A1) are found from the $\Delta_R = 0$ condition, as

$$p = 0 \tag{A2}$$

$$p = \pm i|\xi|C_R$$

where C_R is the Rayleigh wave velocity. The four branch points, at which, $k_\alpha = 0$ and $k\beta = 0$, are given by

$$p = \pm i|\xi|\alpha \tag{A3}$$

$$p = \pm i|\xi|\beta$$

Branch cuts are made as depicted in Fig. 7 such that the integrands in eqn (A1) will be single-valued and analytic on

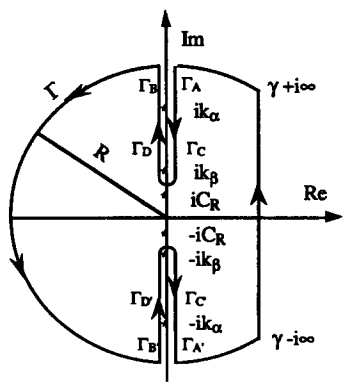

Fig. 7. Integration contour path on the p-complex plane.

$$\bar{u}_{xx}=\frac{-(2c_\alpha c_\beta \mathrm{e}^{-|\xi|c_\beta z}-(2-C_\mathrm{R}^2/\beta^2)\mathrm{e}^{-|\xi|c_\alpha z})(2c_\alpha c_\beta \mathrm{e}^{-|\xi|c_\beta \zeta}-(2-C_\mathrm{R}^2/\beta^2)\mathrm{e}^{-|\xi|c_\alpha \zeta})}{\rho K(C_\mathrm{R})c_\alpha}\frac{\sin^2\xi C_\mathrm{R}t/2}{|\xi|}$$
$$+\int_\beta^\alpha \frac{4c^2(4a^2b^2\sin b(z+\zeta)|\xi|-2abc(\mathrm{e}^{-|\xi|a\zeta}\cos bz\xi+\mathrm{e}^{-|\xi|az}\cos b\zeta\xi))}{\pi\rho a((2-\eta^2/\beta^2)^4+16(\eta^2/\beta^2-1)(1-\eta^2/\alpha^2))\eta^3}\frac{\sin^2\xi\eta t/2}{|\xi|}\mathrm{d}\eta$$
$$-16\int_\beta^\alpha \frac{b(4a^2b^2\cos b(z+\zeta)\xi+2abc(\mathrm{e}^{-|\xi|a\zeta}\sin bz|\xi|+\mathrm{e}^{-|\xi|az}\sin b\zeta|\xi|)-c^2\mathrm{e}^{-|\xi|a(z+\xi)})}{\pi\rho((2-\eta^2/\beta^2)^4+16(\eta^2/\beta^2-1)(1-\eta^2/\alpha^2))\eta^3}\frac{\sin^2\xi\eta t/2}{|\xi|}\mathrm{d}\eta$$
$$-4\int_\alpha^\infty \frac{4a^2b^2\cos b(z+\zeta)\xi+2abc(\cos(bz+a\zeta)\xi+\cos(b\zeta+az)\xi)+c^2\cos a(z+\zeta)\xi}{\pi\rho a((2-\eta^2/\beta^2)^2+4\sqrt{\eta^2/\beta^2-1}\sqrt{\eta^2/\alpha^2-1})\eta^3}\frac{\sin^2\xi\eta t/2}{|\xi|}\mathrm{d}\eta \tag{A5}$$

$$\bar{u}_{zx}=\frac{(2\mathrm{e}^{-|\xi|c_\beta z}-(2-C_\mathrm{R}^2/\beta^2)\mathrm{e}^{-|\xi|c_\alpha z})(2c_\alpha c_\beta \mathrm{e}^{-|\xi|c_\beta \zeta}-(2-C_\mathrm{R}^2/\beta^2)\mathrm{e}^{-|\xi|c_\alpha \zeta})}{\rho K(C_\mathrm{R})}\frac{\mathrm{i}\sin^2\xi C_\mathrm{R}t/2}{|\xi|}$$
$$-\int_\beta^\alpha \frac{4c^2(4ab\cos b(z+\zeta)\xi+2c(\mathrm{e}^{-|\xi|a\zeta}\sin bz|\xi|-ab\mathrm{e}^{-|\xi|az}\cos b\zeta\xi))}{\pi\rho((2-\eta^2/\beta^2)^4+16(\eta^2/\beta^2-1)(1-\eta^2/\alpha^2))\eta^3}\frac{\mathrm{i}\sin^2\xi\eta t/2}{\xi}\mathrm{d}\eta$$
$$-16\int_\beta^\alpha \frac{ab(4ab\sin b(z+\zeta)|\xi|-2c(\mathrm{e}^{-|\xi|a\zeta}\cos bz\xi+ab\mathrm{e}^{-|\xi|az}\sin b\zeta|\xi|)+c^2\mathrm{e}^{-|\xi|a(z+\xi)})}{\pi\rho((2-\eta^2/\beta^2)^4+16(\eta^2/\beta^2-1)(1-\eta^2/\alpha^2))\eta^3}\frac{\mathrm{i}\sin^2\xi\eta t/2}{\xi}\mathrm{d}\eta$$
$$-4\int_\alpha^\infty \frac{(4ab\sin b(z+\zeta)\xi+2c(\sin(bz+a\zeta)\xi-ab\sin(b\zeta+az)\xi)-c^2\sin a(z+\zeta)\xi}{\pi\rho a((2-\eta^2/\beta^2)^2+4\sqrt{\eta^2/\beta^2-1}\sqrt{\eta^2/\alpha^2-1})\eta^3}\frac{\mathrm{i}\sin^2\xi\eta t/2}{|\xi|}\mathrm{d}\eta \tag{A6}$$

$$\bar{u}_{zz}=\frac{-(2c_\alpha c_\beta \mathrm{e}^{-|\xi|c_\alpha z}-(2-C_\mathrm{R}^2/\beta^2)\mathrm{e}^{-|\xi|c_\beta z})(2c_\alpha c_\beta \mathrm{e}^{-|\xi|c_\alpha \zeta}-(2-C_\mathrm{R}^2/\beta^2)\mathrm{e}^{-|\xi|c_\beta \zeta})}{\rho K(C_\mathrm{R})c_\beta}\frac{\sin^2\xi C_\mathrm{R}t/2}{|\xi|}$$
$$+4\int_\beta^\alpha \frac{c^2(4a^2b^2\mathrm{e}^{-a(z+\zeta|\xi|}+2abc(\mathrm{e}^{-|\xi|az}\sin b\zeta|\xi|+\mathrm{e}^{-|\xi|a\zeta}\sin bz|\xi|)-c^2\cos b(z+\zeta|\xi|))}{\pi\rho b((2-\eta^2/\beta^2)^4+16(\eta^2/\beta^2-1)(1-\eta^2/\alpha^2))\eta^3}\frac{\sin^2\xi\eta t/2}{|\xi|}\mathrm{d}\eta$$
$$-16\int_\alpha^\beta \frac{a(c^2\sin b(z+\zeta)|\xi|+2abc(\mathrm{e}^{-|\xi|az}\cos b\zeta|\xi|+\mathrm{e}^{-|\xi|a\zeta}\cos bz\xi))}{\pi\rho((2-\eta^2/\beta^2)^4+16(\eta^2/\beta^2-1)(1-\eta^2/\alpha^2))\eta^3}\frac{\sin^2\xi\eta t/2}{|\xi|}\mathrm{d}n$$
$$-4\int_\alpha^\infty \frac{(4a^2b^2\cos a(z+\zeta)\xi+2abc(\cos(b\zeta+az)\xi+\cos(bz+a\zeta)\xi)+c^2\cos b(z+\zeta)\xi}{\pi\rho b((2-\eta^2/\beta^2)^2+4\sqrt{\eta^2/\beta^2-1}\sqrt{\eta^2/\alpha^2-1})\eta^3}\frac{\sin^2\xi\eta t/2}{|\xi|}\mathrm{d}\eta \tag{A7}$$

$$\bar{u}_{xz}=\frac{-(2\mathrm{e}^{-|\xi|c_\alpha z}-(2-C_\mathrm{R}^2/\beta^2)\mathrm{e}^{-|\xi|c_\beta z})(2c_\alpha c_\beta \mathrm{e}^{-|\xi|c_\beta \zeta}-(2-C_\mathrm{R}^2/\beta^2)\mathrm{e}^{-|\xi|c_\beta \zeta})}{\rho K(C_\mathrm{R})}\frac{\mathrm{i}\sin^2\xi C_\mathrm{R}t/2}{\xi}$$
$$+\int_\beta^\alpha \frac{4c^2(4ab\mathrm{e}^{-|\xi|a(z+\zeta)}+2c(\mathrm{e}^{-|\xi|az}\sin b\zeta|\xi|-ab\mathrm{e}^{-|\xi|a\zeta}\cos bz\xi)-c^2\sin b(z+\zeta)|\xi|))}{\pi\rho((2-\eta^2/\beta^2)^4+16(\eta^2/\beta^2-1)(1-\eta^2/\alpha^2))\eta^3}\frac{\mathrm{i}\sin^2\xi\eta t/2}{\xi}\mathrm{d}\eta$$
$$+16\int_\beta^\alpha \frac{ab(c^2\cos b(z+\zeta)\xi-2c(\mathrm{e}^{-|\xi|az}\cos bz\xi+ab\mathrm{e}^{-|\xi|a\zeta}\sin bz|\xi|))}{\pi\rho((2-\eta^2/\beta^2)^4+16(\eta^2/\beta^2-1)(1-\eta^2/\alpha^2))\eta^3}\frac{\mathrm{i}\sin^2\xi\eta t/2}{\xi}\mathrm{d}n$$
$$+4\int_\alpha^\infty \frac{(4ab\sin a(z+\zeta)\xi+2c(\sin(az+b\zeta)\xi-ab\sin(a\zeta+bz)\xi)-c^2\sin b(z+\zeta)\xi}{\pi\rho((2-\eta^2/\beta^2)^2+4\sqrt{\eta^2/\beta^2-1}\sqrt{\eta^2/\alpha^2-1})\eta^3}\frac{\mathrm{i}\sin^2\xi\eta t/2}{|\xi|}\mathrm{d}\eta \tag{A8}$$

the p-plane. Based on the residue theory, the following holds (see Ref.[21])

$$\int_{\gamma-\infty}^{\gamma+\infty} = 2\pi i \,\text{Res} - \int_{\Gamma} - \int_{\Gamma_A} - \int_{\Gamma_B} - \int_{\Gamma_C} - \int_{\Gamma_D} - \int_{\Gamma_{A'}} - \int_{\Gamma_{B'}} - \int_{\Gamma_{C'}} - \int_{\Gamma_{D'}} \tag{A4}$$

It can be shown that the integrals along the contour Γ become zero as the radius R tends to infinity.

After some manipulations, the expressions A5–A8 are obtained
where

$$K(C_R) = C_R^3\left(\frac{c_R}{\beta^2} - \frac{1}{\alpha^2}\frac{c_\beta}{c_\alpha} - \frac{1}{\beta^2}\frac{c_\alpha}{c_\beta}\right) \tag{A9}$$

and

$$x_j = (-1)^j x \quad (j=0,1) \tag{A10}$$

$$a = \sqrt{|\eta^2/\alpha^2 - 1|} \tag{A11}$$

$$b = \sqrt{|\eta^2/\beta^2 - 1|} \tag{A12}$$

$$c = 2 - \eta^2/\beta^2 \tag{A13}$$

$$c_\alpha = \sqrt{1 - C_R^2/\alpha^2} \tag{A14}$$

$$c_\beta = \sqrt{1 - C_R^2/\beta^2} \tag{A15}$$

$$c_R = 2 - C_R^2/\beta^2 \tag{A16}$$